#### ORIGINAL PAPER



# Permeability Evolution in Natural Fractures Subject to Cyclic Loading and Gouge Formation

Daniel Vogler<sup>1</sup> · Florian Amann<sup>1</sup> · Peter Bayer<sup>1</sup> · Derek Elsworth<sup>2</sup>

Received: 6 September 2015/Accepted: 3 June 2016 © Springer-Verlag Wien 2016

**Abstract** Increasing fracture aperture by lowering effective normal stress and by inducing dilatant shearing and thermoelastic effects is essential for transmissivity increase in enhanced geothermal systems. This study investigates transmissivity evolution for fluid flow through natural fractures in granodiorite at the laboratory scale. Processes that influence transmissivity are changing normal loads, surface deformation, the formation of gouge and fracture offset. Normal loads were varied in cycles between 1 and 68 MPa and cause transmissivity changes of up to three orders of magnitude. Similarly, small offsets of fracture surfaces of the order of millimeters induced changes in transmissivity of up to three orders of magnitude. During normal load cycling, the fractures experienced significant surface deformation, which did not lead to increased matedness for most experiments, especially for offset fractures. The resulting gouge material production may have caused clogging of the main fluid flow channels with progressing loading cycles, resulting in reductions of transmissivity by up to one order of magnitude. During one load cycle, from low to high normal loads, the majority of tests show hysteretic behavior of the transmissivity. This effect is stronger for early load cycles, most likely when surface deformation occurs, and becomes less pronounced in later cycles when asperities with low asperity strength failed. The influence of repeated load cycling on surface deformation is investigated by scanning the specimen surfaces before and after testing. This allows one to study asperity height distribution and surface deformation by evaluating the changes of the standard deviation of the height, distribution of asperities and matedness of the fractures. Surface roughness, as expressed by the standard deviation of the asperity height distribution, increased during testing. Specimen surfaces that were tested in a mated configuration were better mated after testing, than specimens tested in shear offset configuration. The fracture surface deformation of specimen surfaces that were tested in an offset configuration was dominated by the breaking of individual asperities and grains, which did not result in better mated surfaces.

**Keywords** Fracture mechanics · Fracture transmissivity · EGS · Fracture surfaces · Aperture · Gouge

#### 1 Introduction

Anthropogenic intervention and resulting perturbations (e.g., hydraulic fracturing) in a rock mass at great depth may result in complex thermal-hydro-mechanical response. This is of particular relevance when dealing with enhanced geothermal systems (EGS) and unconventional oil and gas extraction utilizing hydraulic fracturing. Our focus here is on EGS, which is considered to be a promising option for generating electricity from hot but naturally low permeable deep formations (Tester et al. 2006). Studying the key THM coupled processes associated with specific reservoir characteristics in an EGS is of foremost relevance to establish a reliable heat exchanger capable of achieving the target production rate while maintaining low background seismicity. The triggering of elevated seismic activity can cause the termination of EGS projects due to damage to

Published online: 20 June 2016



<sup>☐</sup> Daniel Vogler daniel.vogler@erdw.ethz.ch

Department of Earth Sciences, Swiss Federal Institute of Technology Zurich, Sonneggstr. 5, 8092 Zurich, Switzerland

Department of Energy and Mineral Engineering, EMS Energy Institute, Center for Geomechanics, Geofluids, and Geohazards, Pennsylvania State University, University Park, PA, USA

facilities on the surface (e.g., the hot dry rock EGS project in Basel in 2006). Rock transmissivity and flow rates in fractures determine the productivity of geothermal reservoirs and are controlling factors of whether reservoirs are economically feasible. Lowering effective normal stresses by high-pressure injection, dilatant shearing of critically stressed fractures or thermo-elastic effects (e.g., cooling) can cause fracture conductivity to increase (Evans 2005).

To relate mechanical and hydraulic effects in fractures, the mechanical and hydraulic aperture ( $a_{\rm m}$  and  $a_{\rm hyd}$ ) are generally considered separately (Witherspoon et al. 1980; Barton et al. 1985; Esaki et al. 1991; Zimmerman et al. 1991; Park et al. 2013). While the mechanical aperture describes the physical distance between two fracture surfaces, the hydraulic aperture describes the aperture accommodating a particular flux assuming a parallel plate model. With increasing mechanical aperture the hydraulic aperture increases, but the relation between the mechanical aperture and the hydraulic aperture is not one to one (Esaki et al. 1991, 1999; Rutqvist and Stephansson 2003; Xiong et al. 2011 and McClure and Horne 2014).

The common constitutive equations are based on aperture and linearly relate the flow rate in a fracture to the pressure gradient. Fluid flow between parallel walls can be derived from the simplified, incompressible Navier–Stokes equations (Louis 1969), as,

$$Q = -\frac{a_{\rm hyd}^3 w}{12\mu} \nabla p \tag{1}$$

where Q represents the fluid flow rate,  $a_{\text{hyd}}$  the hydraulic aperture, w the fracture width,  $\mu$  the dynamic viscosity and p the fluid pressure.

HM-coupled laboratory investigations reveal that assuming the same mechanical and hydraulic aperture is not generally valid (Raven and Gale 1985; Brown 1987; Cook 1992; Renshaw 1995; Hakami and Larsson 1996; Oron and Berkowitz 1998; Esaki et al. 1999; Chen et al. 2000 and Lee and Cho 2002).

Laboratory tests on granite, marble and basalt specimens with tension-induced artificial fractures by Witherspoon et al. (1980) and on artificial resin fractures by Li et al. (2008) found the approximation of fluid flow with a parallel plate model with an effective hydraulic aperture to be suitable depending on the fracture roughness characteristics. Findings by Raven and Gale (1985), Cook (1992), Hakami and Larsson (1996), Oron and Berkowitz (1998), Esaki et al. (1999), however, showed hydraulic apertures to be consistently smaller than mechanical apertures. Studies by Cook (1992) and by Oron and Berkowitz (1998) showed decreasing mechanical aperture leading to a faster than cubic decrease in hydraulic conductivity and a nonlinear increase in contact area. Zimmerman et al. (1991) demonstrated that the ratio of the hydraulic aperture to the

mean mechanical aperture is related to the ratio of the mean mechanical aperture and its standard deviation. In contrast, Renshaw (1995) found the hydraulic aperture to be constant below a residual hydraulic aperture, while the mechanical aperture could still decrease further when the normal load was increased.

Analysis of experimental data by Cook (1992) and Park et al. (2013) showed mechanical normal joint stiffness and hydraulic aperture to be largely dependent on the contact area between fracture surfaces. Joint stiffness, joint closure and fluid flow were shown to behave highly nonlinearly. Also, as normal loads on a specimen are cycled, hysteretic behavior results. The exponent of the aperture is increasingly higher than cubic with progressive fracture closing.

Experimental work by Durham and Bonner (1994), Esaki et al. (1991), Esaki et al. (1999), Chen et al. (2000), Li et al. (2008), Park et al. (2013) found the hydraulic conductivity of natural fractures to be significantly larger with fracture shear displacements. Esaki et al. (1991, (1999) and Lee and Cho (2002) also found increases in transmissivity to become smaller with ongoing shear displacement. This behavior was controlled by the maximum asperity heights and the distance between asperities. For repetitive forward and reverse shearing, the development of wear products from fracture surface deformation (gouge) was found to decrease transmissivity by an order of magnitude. A commonly used relationship between shear and normal stress to represent changes in conductivity was developed by Barton et al. (1985). This relationship was tested for rock specimens of various sizes and utilizes surface roughness quantities [i.e., the joint roughness coefficient (JRC)] to quantify surface roughness.

While the hydraulic aperture inferred from experiments normally only represents an averaged hydraulic aperture, fracture flow depends on fracture surface heterogeneity, which is also strongly fracture size dependent (Renshaw 1995; Yeo et al. 1998; Oron and Berkowitz 1998; Pyrak-Nolte and Morris 2000; Walsh 2003; Li et al. 2008, 2014; Park et al. 2013).

The findings of previous experiments demonstrate that the cubic law and a linear relation between mechanical and hydraulic aperture are only partially valid, which serves as motivation for this study. In this study, several coupled processes of importance for reservoir modeling are examined for a single fracture. The overall objective is to define the evolution of fracture transmissivity in natural fractures under applied normal and shear displacements as an analog to the response of fracture networks to changes in applied effective stresses driven by fluid pressures and thermal loads. Changes in transmissivity due to changes in confining stress on the specimen are studied for single loading cycles. This includes an analysis of fracture surface damage and the production of gouge material. The experimental setup allows one to compare changes in mechanical and hydraulic aperture during specimen loading.



For increases in confining stress, the effect of the matedness of the two fracture surfaces is examined by performing experiments with well-mated and offset fracture surfaces. This provides qualitative as well as quantitative information on the impact of dilation due to shear displacement, production of gouge material, and quantitative insight into the magnitudes of transmissivity and transmissivity changes during cyclic loading.

#### 2 Methods

#### 2.1 Specimen Preparation

Granodiorite specimens were provided by the Grimsel Test Site, Switzerland. The specimens were obtained from cores of the CRIEPI fractured rock study (Takana et al. 2014). Twelve laboratory specimens with a diameter of 2.5 cm and a length of 6 cm were produced by overcoring preexisting fractures in 10.5 cm cores (Table 1; Fig. 1). The overcoring orientation was chosen so that fractures are aligned parallel to the specimen's main axis. The fractures were classified as tensile (mode I) and shear (mode II) fractures (Table 1). Classification of the fracture type was performed by investigating fracture surfaces for slickensides, plumose structures, mineralization and crack propagation through individual grains.

#### 2.2 Experimental Setup

The experimental setup consisted of a pressure-tapped core holder of the DCH series (Fig. 2, Table 2), as produced by Core Lab. The core holder setup was described in detail by Wang et al. (2011).

Table 1 Physical properties of the specimen under investigation with original specimen length, shear displacement offset, the resulting effective specimen length and the distinction between tensile and shear fracture mode

Test specimen (-)	Specimen length (mm)	Shear offset (mm)	Eff. length (mm)	Frac. mode (–)
1	61	0	60	I
2	62	0	60	II
3	62	0	60	I
4	60	0	60	I
5	60	2	58	I
6	60	2	58	I
7	60	3	57	I
8	61	3	58	I
9	60	6	54	I
10	62	5	57	II
11	60	1	59	I
12	60	1	59	I

One Isco pump (model 500D; pump  $P_A$ ) and two Isco pumps (model 100DM; pumps  $P_B$  and  $P_C$ ) were utilized to control the fluid pressure at the specimen inlet  $p_{fp}$  (pump  $P_C$ ), the confining pressure  $p_{co}$  (pump  $P_B$ ) and to measure



Fig. 1 Example of overcored specimen on top of one fracture surface

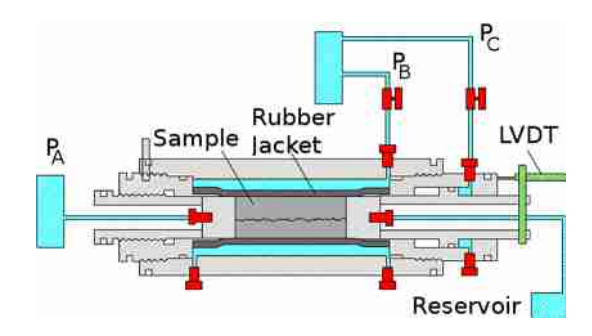


**Fig. 2** Experimental setup of core holder and specimen. The pressures were prescribed in pumps  $P_A$  (axial pressure  $p_{ax}$ ),  $P_B$  (confining pressure  $P_{co}$ ) and  $P_C$  (fluid inlet pressure  $p_{fp}$ )

**Table 2** Pumps used in the setup with model, minimum and maximum pressures  $p_{\min}$  and  $p_{\max}$ , standard pressure accuracy SPA

	$P_A \ p_{\mathrm{fp}}$	$P_B \ p_{ m co}$	$P_C$ $p_{ax}$
Model (–)	500D	100DM	100DM
Min. pressure (MPa)	0.67	0.67	0.67
Max. pressure (MPa)	25.9	69	69
Volume (mL)	507	103	103
SPA (% FS)	0.1	0.1	0.1

the axial pressure  $p_{\rm ax}$  (pump  $P_A$ ). Similar setups for investigation of rock specimen properties were employed by Zhu et al. (2007), Wang et al. (2011), Shugang et al. (2013) and Zhong et al. (2014), but focusing on different research questions.

The specimen placement with the fracture oriented parallel to the core holder axis produces fluid flow along the fracture from the inlet to the outlet. Specimens were loaded with an initial confining stress of 1 MPa, and steady-state flow was established. At all times, the fluid pressure at the outlet was kept at atmospheric pressure  $p_{\text{atm}}$ and the inlet pressure was recorded. When initial equilibrium of fluid pressure for a given flow rate was reached, the confining stress was increased incrementally by 1-2.5 MPa up to a maximum of 68 MPa and subsequently decreased back down to 1 MPa, thereby completing one loading cycle. After each incremental increase in confining stress, the confining stress was kept constant until the fluid inlet pressure necessary to maintain a constant flow rate Q through the specimen reached a steady-state condition. During the experiment, the flow rate Q was kept constant for individual loading cycles. Accuracy of flow rate measurements was 0.5 % of setpoint (i.e., the currently read pressure in the pump). Between 5 and 10 loading cycles were performed for each specimen.

## 2.3 Permeability Behavior of Natural Fractures Under Various Loading Scenarios

The experimental setup was used to test transmissivity changes of natural fractures under changing confining stress conditions. Confining stress is applied radially on the cylindrical specimen. The fracture surfaces were investigated in mated and offset configurations with offsets among fracture surfaces ranging between 1 and 6 mm. An example of open and closed fractures is shown in Fig. 3. Offset of the fractures occurred in the axial direction. Differentiating between mated and offset fracture surfaces enabled us to investigate the effect of shear displacement on transmissivity and surface deformation.



Fig. 3 Example of overcored specimen a open and b closed

The main measured properties are the inlet fluid pressure  $p_{\rm fp}$  and the confining pressure  $p_{\rm co}$ . The effective confining pressure  $p_{\rm co,eff}$  was calculated by

$$p_{\text{co,eff}} = p_{\text{co}} - \frac{p_{\text{fp}} + p_{\text{atm}}}{2} \tag{2}$$

A representative transmissivity T was derived from the cubic law (Eq. 1) to allow one to investigate changes in transmissivity, with the transmissivity being independent of changes in flow rate in subsequent cycles. If the flow rate Q is changed between load cycles, the representative transmissivity T does not change if the changes in pressure gradient  $\nabla p$  are proportional to the changes in flow rate.

$$Q = \frac{a_h^3 * d}{12u} \nabla p \tag{3}$$

$$T = \frac{a_h^3}{12\mu} = \frac{Q}{d\nabla p} = \frac{Q}{d}\frac{\Delta L}{\Delta p} \tag{4}$$

where d is the specimen diameter,  $a_h$  is the hydraulic aperture, p the flow pressure and  $\mu$  the dynamic viscosity of water. The transmissivity T is used to make a comparison between individual experiments because T relates the flow rate driven by a unit pressure gradient, rather than a head gradient in the normal hydrogeological definition. Note that the transmissivity T is related to the normal hydrogeological definition of transmissivity  $T_h$  as  $T_h = T\gamma$  where  $\gamma$  is the unit weight of the flowing fluid. Reporting the transmissivity offers the advantage of reporting all properties known in the experiment (e.g., Q,  $\Delta L$ ,  $\Delta p$  and d) in one variable. This allows straightforward comparison of experiments performed with different flow rates Q or on fractures with varying width d. Similar forms of the transmissivity were also used in Renshaw (1995), Gentier et al. (2013) and Zimmerman and Bodvarsson (1996).

Besides the hydraulic analysis, surface deformation was determined and mineralogical characterization of the fracture surfaces was performed.

#### 2.4 Surface Scans

Prior to testing, replicas of the fracture surfaces were produced. These were utilized to obtain high-resolution photogrammetric scans of the surface. Fracture surfaces were evaluated with surface scans recorded with the ATOS



Core 3D scanner from GOM. The ATOS Core sensor projects fringe patterns on the object surface, which are recorded by two cameras. The patterns form a phase shift that is based on a sinusoidal intensity distribution which enables one to calculate the three-dimensional (3-D) surfaces. The photogrammetry scanner is calibrated with two tests. The diameter and shape of a sphere and the distance between two spheres that are mounted on a plate are measured with the photogrammetry scanner to derive calibration errors and accuracy. All equipments used for calibration are specifically developed by the company GOM, which manufactures the scanner. The photogrammetry scanner was calibrated with length deviation errors between 0.009 and 0.027 mm and optimized calibration deviations of 0.014  $\pm$  0.001 pixels.

The same process was repeated for the damaged surfaces after testing to analyze the surface changes that occurred during the experiments and compare these to the changes in transmissivity during the experiment. Surface damage during testing caused gouge material to accumulate in the fracture planes. Analyzing the gouge material found in the fracture after testing can give insight into possible relations between the grain size distribution of the gouge material and transmissivity changes during mechanical cycling.

A similar analysis is performed by computing the asperity distributions on the fracture surfaces derived from the fracture scans before and after the tests. The changes on the fracture surfaces can also be used to determine probable relations to transmissivity changes during testing.

## 2.5 Grain Size Analysis

The grain size distribution of the gouge material produced during testing was measured by sieving samples larger than 1 mm and by using laser spectrometry (Malvern Instruments Mastersizer 2000) for all gouge material below 1 mm. The gouge material is analyzed for volumetric distribution of gouge instead of weight. This is done because laser spectrometry allows a very accurate measurement of grain size volume down to around 10 micrometers.

#### 2.6 Aperture Changes

The volume change of the confining fluid during cyclic loading was recorded in each experiment and was used to calculate the volumetric strain. After removing noise and accounting for confining pressure changes, these data were used to quantify relative mechanical aperture changes during cycling, assuming that the volume change is entirely associated with fracture deformations.

When rubber jacket and specimen volumes decrease (Fig. 2), the pump controlling the confining pressure has to

adjust for this increase in volume of the confining pressure fluid. The volume of the rubber jacket can decrease due to deformation of the jacket and the specimen enclosed within. The rubber jacket itself deforms elastically, which allows one to separate the volumetric changes of the rubber jacket and the specimen. These changes can be attributed to the elastic deformation of the specimen itself as well as to reversible and permanent changes of the fracture. To calibrate this, an additional test with an intact granodiorite specimen was performed for loading between 1 and 68 MPa. Therefore, the changes in confining fluid volume  $d(V_{p,\mathrm{conf}})$  are related to the changes in mechanical aperture  $da_{\mathrm{mech}}$  by

$$da_{\text{mech}} = \frac{dV_{p,\text{conf}}}{d \times l} \tag{5}$$

where d is the specimen diameter and l is the specimen length. The change in hydraulic aperture derived from fluid pressure increase can be compared to the mechanical aperture decrease, and the hydraulic aperture can be calculated with Eq. 3. Changes in hydraulic aperture are measured by comparing the hydraulic aperture during the experiment to the initial value at the start of the experiment with 1 MPa confining pressure.

#### 3 Results

In the performed experiments, we measured the fluid pressure gradient response to changing confining pressure on a natural fracture. The flow rate Q was kept constant for individual cycles, and the required fluid pressure gradient  $\nabla p$  to maintain Q was measured. A representative fracture conductivity can be calculated in form of the transmissivity (Eq. 4). Hence, transmissivity is used to quantify fracture conductivity changes during the experiments. This section reports on the effect of cyclic loading on the fluid flow, gouge material and the surface damage that can be evaluated after completion of the experiments. To investigate the effect of shear displacement on cyclic loading, two classes of tests were performed on specimens with mated surfaces (tests 1, 2, 3, 4) and on specimens with shear displacement of 1-6 mm (tests 5, 6, 7, 8, 9, 10, 11, 12). A detailed discussion follows in the subsequent Sect. 4. The feasible number of loading cycles was determined for each specimen and the experimental device. Due to the large opening of a natural fracture in comparison with a saw-cut fracture, each specimen was wrapped in a smaller jacket within the larger rubber jacket separating the specimen from the confining fluid. Nonetheless, rupture of the rubber jacket led to the termination of some tests and a maximum of 10 cycles was performed to limit wear on the material. Other reasons for termination of experiments were failure of the



specimen under high normal loads and fluid inlet pressures above 30 MPa. It should be noted here that the effective confining stress in these extreme cases was very variable along the specimen axis, due to the large pressure gradients observed between inlet and outlet. The equilibration times for fluid pressures strongly varied depending on the fracture opening, existing gouge material and applied confining pressures. These times ranged from minutes up to multiple hours for individual changes in confining pressure that were between 1 MPa for small pressures (i.e., 1–10 MPa) and 2.5 MPa for larger pressures (i.e., 10–68 MPa).

Experimental data that are used for further analysis include volume changes, time and pressures that are measured at each pump for confining and fluid flow pumps (Fig. 2). Transmissivity (Eq. 4) and effective confining pressure are chosen to represent the experimental data. Changes in surface properties are characterized by changes in asperity height and the standard deviation of asperity height. These are obtained from inspection of the surface scans. For a concise description of results, we select only experiments 1, 2, 4, 7 and 10 (Fig. 4a-e). The selected experiments are considered representative of hysteretic behavior during normal load increase and transmissivity changes with ongoing cycling. Tests 2 and 4 (Fig. 4b, c) display strongly hysteretic fluid inlet pressures, which are linearly related to the transmissivity. Specimens 2 and 4 were tested in a mated configuration. Specimens 7 and 10 were tested in an offset configuration (3 and 5 mm, respectively) and show hysteretic fluid pressures responses for late cycle numbers (e.g., cycles 4 and later for tests 7 and 10) as well.

#### 3.1 Permeability Changes During Load Cycling

Figure 4a–e depicts the transmissivity changes as derived from Eq. 4 for changing effective confining pressure. The color coding of the data curves ranges from the first cycle (dark red) to the last cycle (dark blue), and the increasing confining pressure path of a cycle is marked with a >, while the decreasing confining pressure path is marked with a <. The general trend shows fracture transmissivity decreasing with increasing cyclic loading (Fig. 4a–c). During the first initial cycles, transmissivity declines rapidly and converges toward later cycling.

Most experiments (Fig. 4b–e) display hysteretic behavior during cycling as fracture transmissivity is lower during unloading of the specimen than during loading. The cyclic loading also allows one to compare transmissivity decrease due to changes in confining stress and increasing cycling and accompanying surface damage. During experiment 1 (Fig. 4a), transmissivity decrease due to larger confining stresses during individual test cycles is on the same order of magnitude as decreases due to irreversible fracture

closure (e.g., due to surface damage) with repeated load cycling. Load cycle 4 shows exceptional behavior with significantly larger initial transmissivity decreases than all other cycles. This is likely related to clogging of a main flow channel in the fracture or clogging of the fluid pipes upstream or downstream of the specimen. The effect of changing confining stress during individual cycles is more pronounced for experiments 2 and 4 (Fig. 4b, c) where transmissivity decreases strongly during initial confining pressure increase and converges against a constant transmissivity value between 10 and 20 MPa effective confining pressure.

In experiment 10 (Fig. 4e), the fracture aperture is very large and the pressure gradient is quite small until 47.5 MPa confining pressure is reached. The fluid pressure gradient then rises quickly, which means that transmissivity is decreasing quickly.

Depending on the surface of the fractures, different response patterns of the transmissivity to increased confining pressure can be observed. Specimen 1 (Fig. 4a) exhibits a small slope that is almost linear on a semilog plot, which stands in stark contrast to specimens 2 and 4 (Fig. 4b, c). The surface of specimen 1 shows significant mineralization and slickensides (Sect. 1) with two wellmated surfaces with a uniform distribution of contact area. While this leads to almost no hysteretic effects between the increasing and decreasing confining stress paths, it also causes a significantly less steep transmissivity decline for small confining stress (1-10 MPa). Tests with shear offset show higher transmissivities (Fig. 4d, e). The large range of transmissivity values for respective confining stresses can also be observed for all specimens in Fig. 13. While increased confining stress and surface damage cause transmissivity values for individual specimen to vary up to three orders of magnitude, the offset of the specimen only seems to have an effect up to 1 mm. For offsets between 1 and 6 mm, the total transmissivity range is comparable for all tests.

#### 3.2 Aperture Changes

Measurements during the experiments only allow one to deduct changes in mechanical aperture, as absolute values are not locally known and measured changes are represented as averages across the whole specimen. Therefore, changes in the mechanical and hydraulic aperture from the starting value of each cycle at 1 MPa confining stress are presented. As both aperture values generally decrease from their starting value at 1 MPa, positive aperture changes denote a reduction of the mechanical or hydraulic aperture. After maximum effective confining stress is reached, the mechanical aperture changes generally decrease, indicating fracture opening. Changes in mechanical and hydraulic



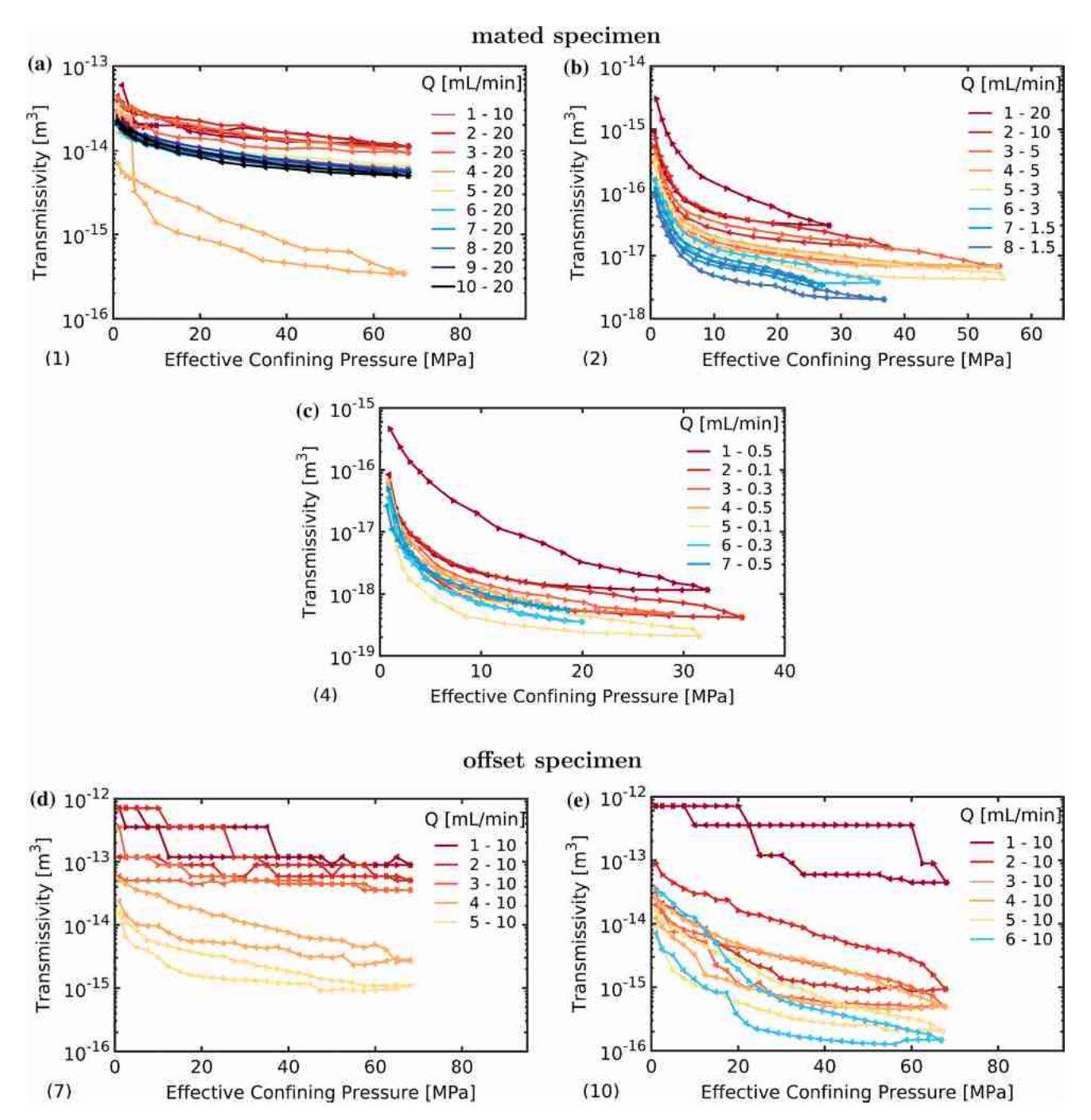


Fig. 4 Tests 1, 2, 4, 7 and 10 are shown in subfigures a—e, respectively. The plots show transmissivity (Eq. 4) versus effective confining pressure. The first number in each row in the legend denotes the cycle number, with *color coding* of the data curves going from the first cycle (*dark red*) to the last cycle (*dark blue*). The second number

in each row in the legend denotes the flow rate during the respective cycle in (mL/min). The curve from 1 MPa to maximum effective confining pressure is marked with  $\triangleright$  while the reverse curve is marked with  $\triangleleft$  (color figure online)

aperture are compared in Fig. 5a–d. As for Fig. 4a–e, stages in the experiment with equilibrated confining and injection pressures are displayed with ▷ and ▷ during increasing and decreasing confining pressure, respectively. Closely spaced markers, therefore, indicate small changes during one confining pressure interval change (2.5 MPa)

while markers spaced further apart indicate rapid changes with confining pressure changes.

The first cycle is not always shown for reasons given below. The specimen and the experimental equipment (i.e., the rubber jacket, see Fig. 2) deform during the first cycle, which can lead to erratic aperture changes. This behavior



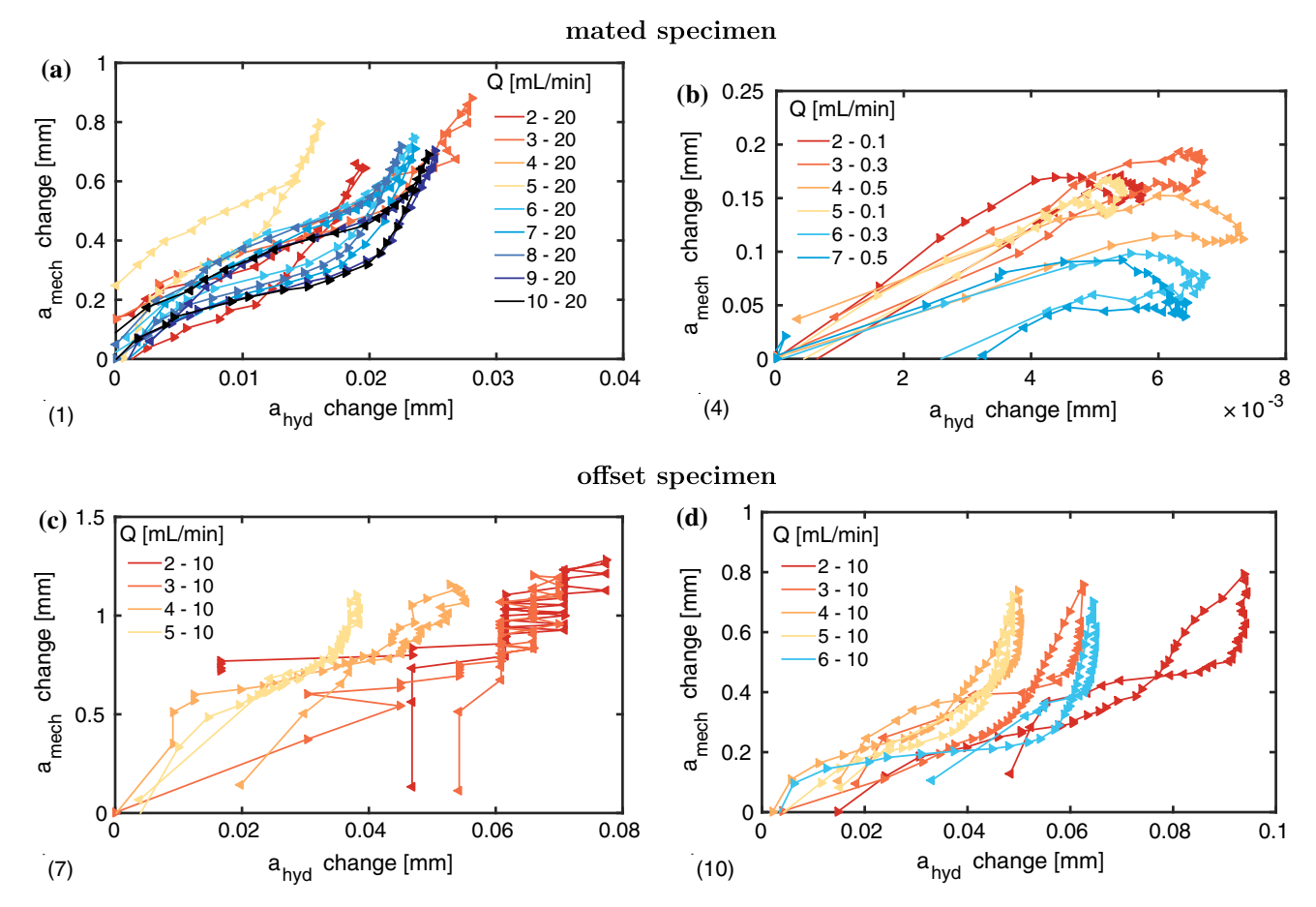


**Fig. 5** Mechanical versus hydraulic aperture changes. Changes are calculated by comparison with the initial values at 1 MPa. Specimens from tests 1, 4, 7 and 10 are assigned to **a–d**, respectively. The curve

from 1 MPa to maximum effective confining pressure is marked with  $\triangleright$  while the reverse curve is marked with  $\triangleleft$ 

can be especially pronounced for the offset specimens where the two fracture sides have a small contact area. Small shear displacements at high confining stresses can lead to rapid fracture normal closure. For offset fracture surfaces (eg., tests 7 and 10), oscillating behavior and rapid changes during initial loading cycles are especially pronounced, due to large initial apertures and fluid flow pressure oscillations.

During test 1, mechanical aperture changes are more than one order of magnitude larger than hydraulic aperture changes (Fig. 5a). For each cycle, the hydraulic aperture changes increase initially drastically until they start to converge. Hydraulic aperture changes for test 4 (Fig. 5b) are also significantly smaller than mechanical aperture changes. Maximum mechanical aperture changes decrease with ongoing load cycling while maximum hydraulic aperture shows no distinct trend. Mechanical aperture changes (i.e., fracture closure) are largest for test 7 (i.e., a specimen that contained a fracture that was tested with 3-mm offset, Fig. 5c). For test 10 (5-mm offset), mechanical aperture initially changes drastically, marked

by wide marker spacing. While mechanical aperture change increases further as the fracture closes, hydraulic aperture changes start converging.

For all tests, maximum mechanical aperture changes (i.e., maximum mechanical aperture closure) remain comparable between cycles (around 1 mm except for test 4 shown in Fig. 5b with 0.2 mm). The mechanical aperture changes of tests 1, 4, 7 and 10 can also be interpreted when comparing mechanical aperture changes to effective confining pressure (Fig. 6a-d). All tests show larger mechanical aperture changes during initial loading (up to 10 MPa), which become smaller for higher effective confining stresses. Other visible trends include small decreases of mechanical aperture changes with ongoing load cycles and hysteretic behavior of mechanical aperture changes. For all tests, the mechanical aperture change is larger than the hydraulic aperture change after the maximum effective confining pressure has been reached and confining stress is decreasing (Fig. 5a-d). Hysteretic effects are more pronounced for mated specimen (Fig. 5a-b), but are still observable for offset specimen (Fig. 5c-d).



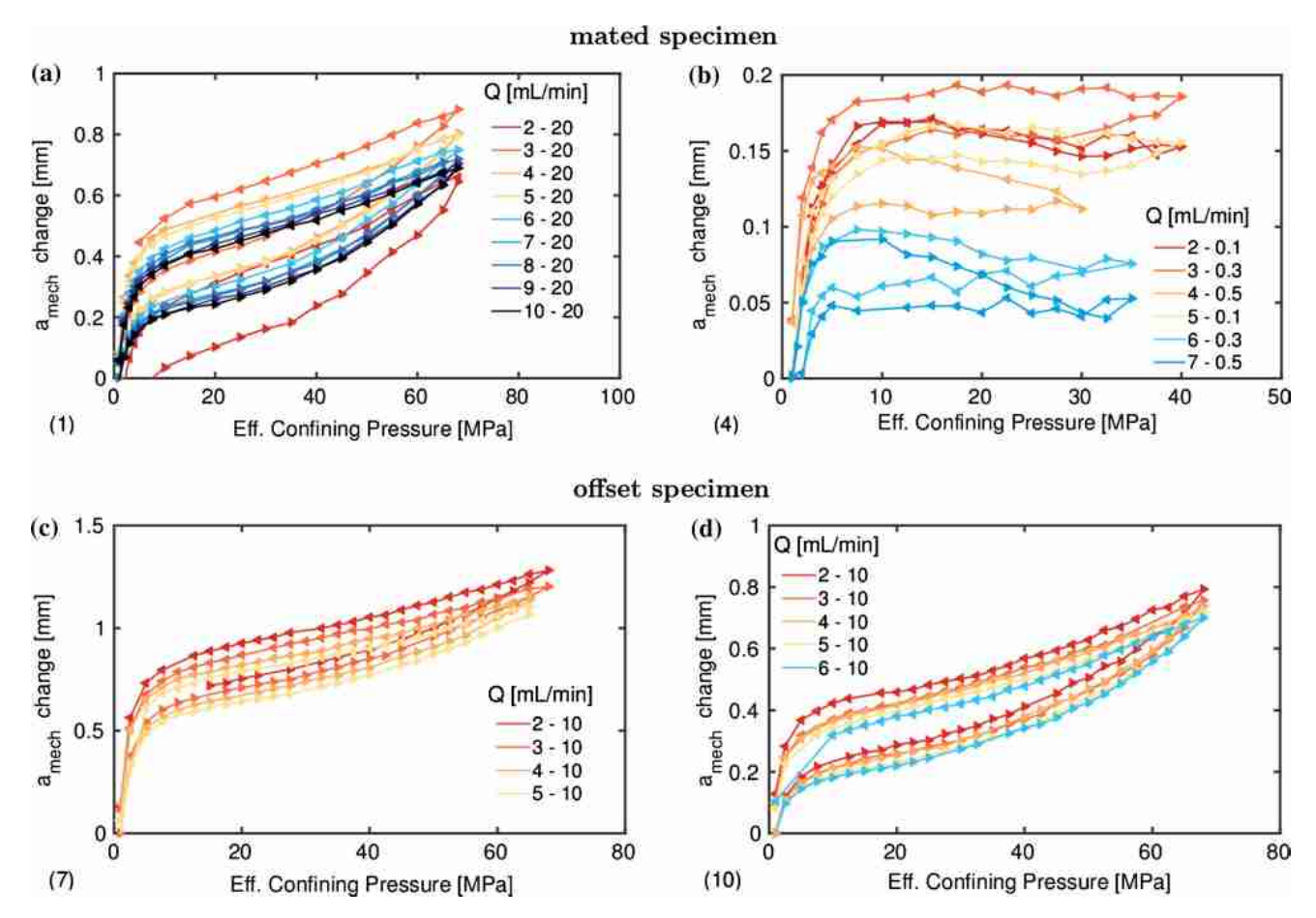


**Fig. 6** Mechanical aperture changes versus effective confining pressure. Changes are calculated by comparison with the initial values at 1 MPa. Specimen from tests 1, 4, 7 and 10 are assigned to

 $\mathbf{a-d}$ , respectively. The curve from 1 MPa to maximum effective confining pressure is marked with  $\triangleright$  while the reverse curve is marked with  $\triangleleft$ 

Here, it should be noted that for tests depicted in Figs. 5a–d and 6a–d, only test 4 (Figs. 5b, 6b) experienced fluid inlet pressures high enough to cause significant differences between the confining stress and effective confining stress.

#### 3.3 Analysis of Gouge Material

Due to the experimental setup, fine and coarse grain material was not collected at the outflow end of the experiment. The gouge material collected after testing was analyzed under a magnifying lens, which found the minerals quartz, feldspar, biotite and chlorite, all common in granodiorite. Specimens 2 and 10 showed slickensides.

The collected volume of gouge material (Fig. 7) follows a log-normal distribution. Since the tests in mated configuration did not lead to significant surface damage, the amount of gouge material was not sufficient to derive a distribution for specimens without shear offset. Specimen 7 had whole individual grains of rock breakouts with sizes up to 6 mm that were not monominerals. Larger quartz

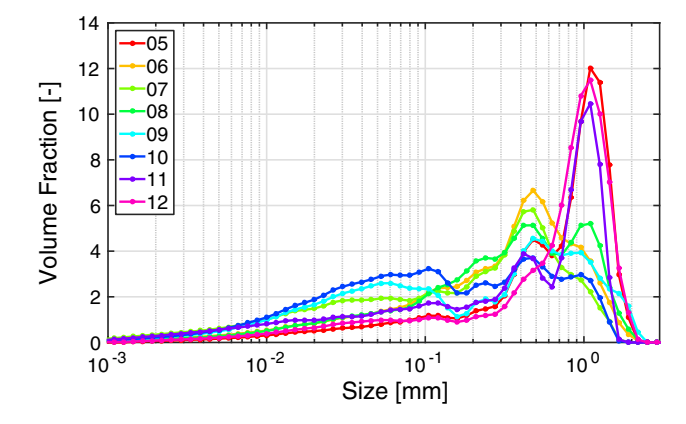


**Fig. 7** Grain size distribution of gouge material for tests 5, 6, 7, 8, 9, 10, 11 and 12

crystals were the dominant minerals on the fracture surface of specimens 1 and 7. Overall, mineral distributions on the fracture surface and of the gouge material revealed to be comparable and did not differ largely for individual specimens and between all specimens. No mineralogical



features larger than the average grain sizes exist in the tested specimens. Changes in transmissivity during normal load cycling are more likely connected to the surface geometry and the specimen offset than the mineralogy of the specimen. This is supported by comparable grain size distributions across tests (Fig. 7). While mineralogy on fracture surfaces was comparable across specimens, changes in transmissivity during cyclic changes in confining stress showed strong correlation to shear offset during testing (Fig. 4a–c for mated specimens versus Fig. 4d–e for offset specimens and Fig. 13).

Larger rock pieces and individual grains that broke off stayed in place during all tests. Smaller grains and fine material were found evenly distributed across the fracture after testing. Therefore, while larger breakouts of material led to stronger surface alteration, fine material is more likely to clog flow channels with gouge that leads to increasing pressure gradients to maintain flow rates.

# 3.4 Comparison of Surface Scans Before and After Testing

Due to the large maximum confining pressures, significant surface deformation was expected in the fracture plane of the specimens. For detailed analysis, photogrammetric surface scans of the fracture specimens were generated before and after the experiments.

The surface scans of the individual sides can be matched to derive the fracture aperture by calculating the distances between the two surface sides. This is fundamental to study the effect of surface roughness, connectivity and the correlation length of the fracture surfaces as well as the respective aperture, which is especially crucial for fracture transmissivity.

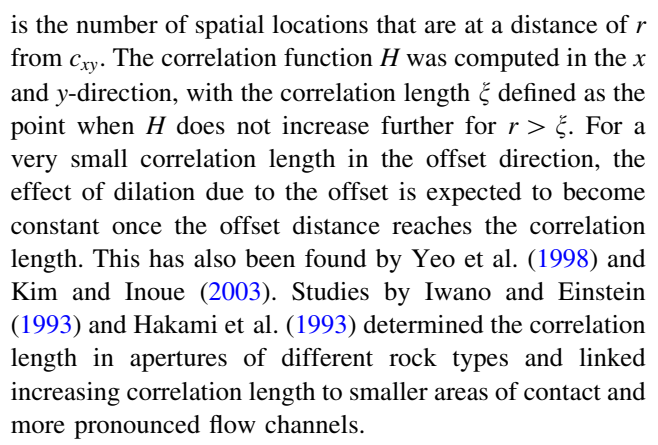
Surface roughness can be quantified with the standard deviation  $h_{\text{std}}$  of the asperity height h in a distribution with an average (mean) asperity height  $h_{\text{ave}}$ .

$$h_{\rm std} = \sum_{i=1}^{N} \frac{(h_{\rm ave} - h_i)^2}{N}$$
 (6)

Another measure to characterize surface roughness is the correlation length of the asperity height, which gives an indication of the directional dependence that is to be expected for shear displacement, which affects fluid flow through the fracture. The correlation length  $\xi$  can be found by studying the convergent behavior of the function H, which is defined as

$$H = \frac{\sum_{i=1}^{n} (z(c_{xy}) - z(c_{xy} + r))^{2}}{n}$$
 (7)

where  $c_{xy}$  is the spatial coordinate in the x- and y-direction on the fracture surface, z is the asperity height at  $c_{xy}$  and n



The asperity distribution before and after testing shows drastic changes when comparing the ranges observed for the cumulative density functions of asperity height distributions on the fracture surfaces (Fig. 11). Figure 11 shows more comparable distributions of asperity heights across all fracture surfaces before testing, with asperity height distributions becoming more heterogeneous after testing when compared between all tested specimens. Photogrammetric scans produced profiles of the surfaces, which were oriented according to a best-fit plane in the x-y coordinates. Therefore, the mean asperity height is close to 0 (Figs. 8, 9). However, for visualization and comparison, an asperity height of 0 mm is assigned to the lowest point of the surface for Fig. 11. While asperity distribution for individual specimens is similar to both fracture surfaces before testing, the two sides show different distributions after testing. This can be attributed to surface damage at individual contact points occurring on the specimen side with the lower asperity strength.

Surface damage also caused the measured correlation lengths to change (Table 3). While the correlation function tended to converge slightly slower for the mated tests (tests 1–4), convergence was changed more significantly for offset tests, with the correlation length increasing (e.g., tests 7 and 8), or even decreasing for one of the surfaces (e.g., surface B in test 9). An example of the correlation length function in *x*-and *y*-direction for specimen 6 is shown in Fig. 12.

Transmissivity values for the maximum effective confining pressure (varies between experiments) and for 1 MPa after each load cycle are shown in Fig. 13a, b, respectively. The marker size changes from early cycles (small circle) to later load cycles (large circle), which enables one to observe quantitative changes of the transmissivity with ongoing load cycles and shear displacement. The impact of effective confining pressure is more pronounced for mated fractures. This becomes apparent when comparing Fig. 13a, b, where specimen with shear offset show transmissivity changes between maximum effective confining stress and at 1 MPa confining stress of one order of magnitude or smaller. Specimens in mated configuration, however, can show



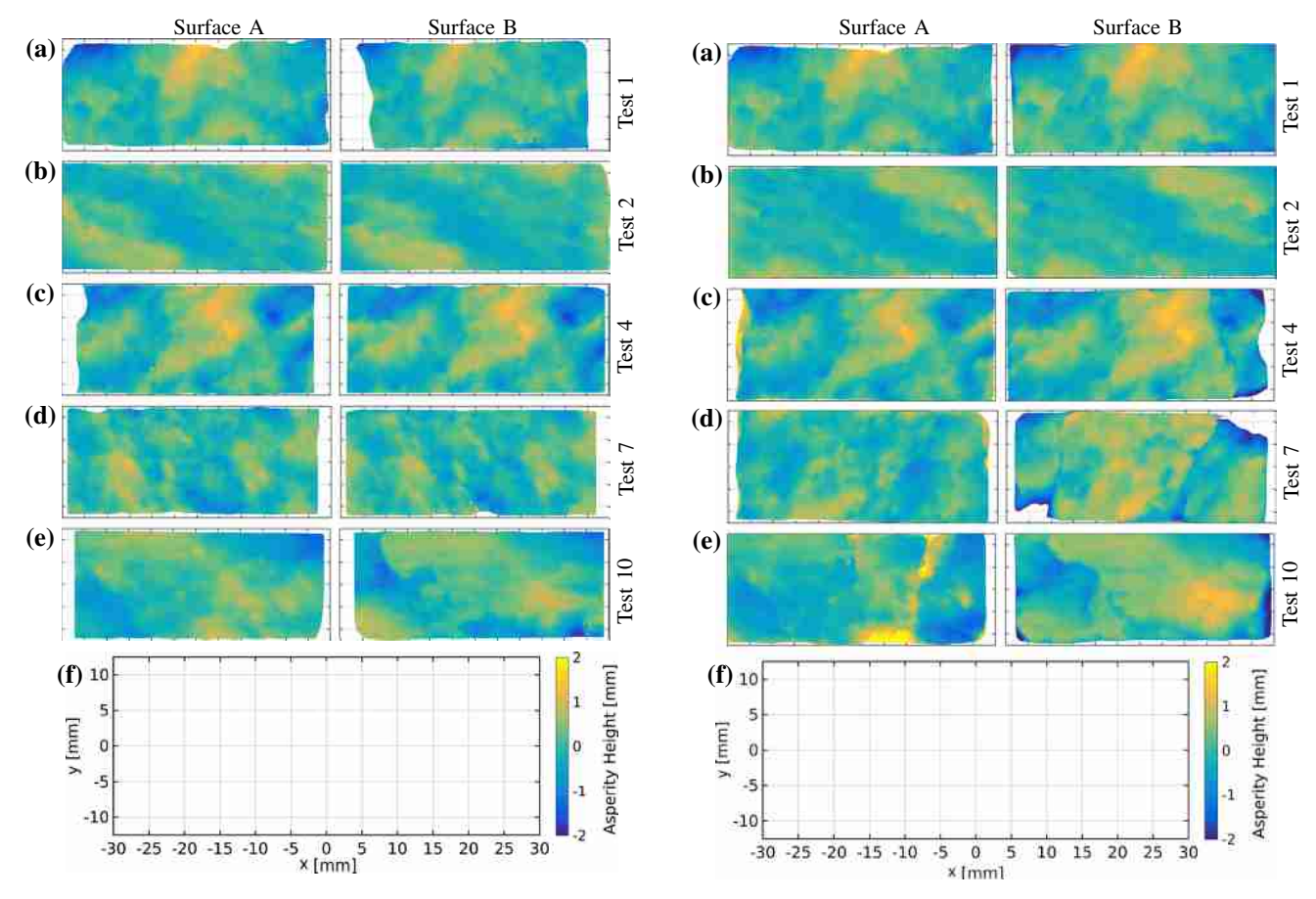


**Fig. 8** Surface scans before testing. Specimens from tests 1, 2, 4, 7 and 10 (*top to bottom*, **a–e**) with surfaces A (*left*) and B right before testing. A reference figure for the surface scan dimensions and asperity height *colorbar* is shown in **f** (color figure online)

**Fig. 9** Surface scans after testing. Specimens from tests 1, 2, 4, 7, 10 (*top to bottom*) with surfaces A (*left*) and B (*right*) before testing. A reference figure for the surface scan dimensions and asperity height *colorbar* is shown in **f** (color figure online)

transmissivity differences of up to two orders of magnitude (e.g., specimens 3 and 4 in Fig. 13a, b). The transmissivity behavior at maximum effective confining stresses does not appear to be influenced by additional shear offset past 1 mm in Fig. 13a, while there is a trend of increasing minimum transmissivity values for 1 MPa effective confining pressure after cycling (Fig. 13b). The general trend of transmissivity decrease for ongoing load cycling is evident in all specimens at maximum effective confining stress and at 1 MPa confining stress after each cycle, with changes in magnitude varying from half an order of magnitude (test 1, 0 mm shear displacement) to three orders of magnitude (test 6, 2 mm shear displacement).

#### 4 Discussion

#### 4.1 Fracture transmissivity

Two fundamental behaviors were observed during this study. First, in the case of mated fractures the

transmissivity decreases rapidly during individual load cycles for effective confining stresses below 10 MPa (Fig. 4a-c). The minimum transmissivity observed during each cycle only shows small changes significantly below one order of magnitude between cycles. However, the minimum transmissivity generally decreases with an increasing number of load cycles (Fig. 4a-c). Secondly, in the cases of offset fractures, the transmissivity does not always decrease significantly during individual cycles, with maximum differences between subsequent cycles of one order of magnitude or lower (Fig. 4d, e). Exceptions are cycles 2 and 6 in experiment 10 (Fig. 4e). Changes of minimum transmissivity between cycles were more pronounced than for individual cycles and mated specimen, with observed changes of multiple orders of magnitude (Fig. 4d, e).

The fact that fault gouge was produced (Fig. 7) during cyclic loading suggests that the transmissivity decrease in both cases is associated with the transport of fault gouge material downstream after surface damage occurred.



**Table 3** Correlation length in direction of the specimen axis (X) and normal to axial direction (Y) before and after testing for fracture surfaces A/B of each specimen, respectively

Test	Pre	Pre	Post	Post
Specimen	X	Y	X	Y
(-)	(mm)	(mm)	(mm)	(mm)
1	24, 19	+, +	27, 28	+, +
2	21, 20	14, 14	25, 24	12, 12
3	28, 26	13, +	27, 28	12, 12
4	16, 18	08, 10	17, 21	10, 11
5	20, 21	10, 10	20, 21	09, 11
6	25, 23	15, +	26, 25	13, +
7	07, 07	13, 08	15, 20	+, +
8	08, 08	09, +	09, 24	09, +
9	25, 26	+, +	27, 19	+, +
10	+, +	14, 12	15, +	+, +
11	22, 20	+, +	25, 20	+, +
12	16, 18	08, 10	17, 21	10, 11

Correlation lengths that did not converge over half of the total length in x- and y-direction are marked with a +

Gouge material transport likely occurs during decreasing confining pressures when the fracture aperture increases again and gouge material that was previously lodged in place can be transported downstream. This observed gouge material production could potentially cause the observed hysteretic behavior by subsequently clogging flow paths, thus lowering fracture transmissivity (Fig. 4b–e).

The results for the mated fractures in Fig. 4 show that most of the transmissivity changes between load cycles occured during the initial cycling (Fig. 4a-c). Mated specimen have more contact area, which can be seen in their aperture fields (Fig. 10a-c). This likely leads to less surface damage as indicated by the small gouge production measured for mated specimen (Fig. 7). The smaller changes observed in transmissivity behavior between load cycles for mated specimen could therefore be linked to less pronounced surface damage. During individual cycles, high effective confining stresses greater than 20 MPa (Fig. 4b, c) do not lead to further transmissivity decrease for mated specimens. As mechanical aperture changes were recorded for effective confining stresses above 20 MPa, this indicates that additional changes in mechanical aperture (Fig. 6a, b) do not affect fluid flow. One possible explanation for this is a crucial change in flow regime from distributed flow across the whole specimen width to channelized flow. This hypothesis is supported by the converging hydraulic aperture changes while mechanical apertures are still decreasing (Fig. 5a, c, d). The slow decrease in transmissivity observed in specimen 1 (Fig. 4a) is in contrast to specimens 2 and 4 (Fig. 4b, c). The aperture fields (Fig. 10a-c) obtained from specimens before and after testing give indications that this

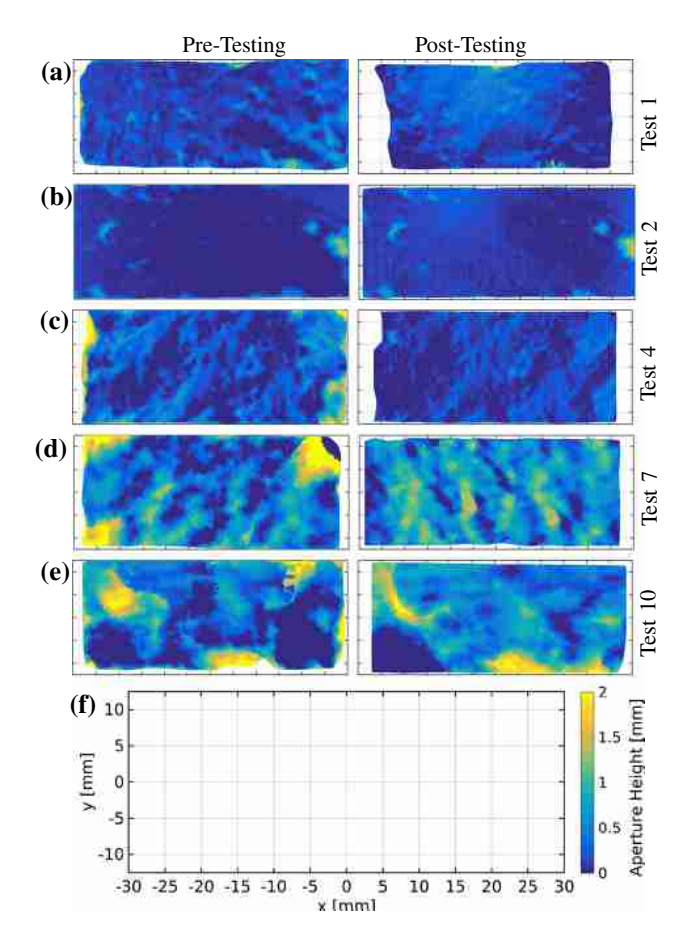


**Fig. 10** Aperture fields as derived from surface scans (Figs. 8, 9). Specimens from tests 1, 2, 4, 7 and 10 ( $top\ to\ bottom$ ) with apertures before (left) and after (right) testing. Reference figure for the aperture field dimensions and aperture size colorbar is shown in  $\mathbf{f}$  (color figure online)

could also be related to surface damage. When comparing aperture fields before and after testing for specimen 1, there is no significant aperture decrease across the fracture (Fig. 10a). Specimen 2 is a shear fracture and has smaller aperture values across the fracture than other specimens, both before and after testing (Fig. 10b). Significant surface damage in form of a reduced aperture across the fracture is apparent for specimen 4, however (Fig. 10c). Observed magnitudes in transmissivity changes during cyclic loading could therefore potentially be strongly linked to the specific fracture and corresponding aperture field configurations (Fig. 13a, b).

Transmissivity changes during load cycles are not as pronounced for shear offset specimens. However, shear offset specimens experience large transmissivity changes between cycles. For shear offset fractures, the aperture fields with small regions of low aperture suggest larger contact stresses between the fracture surfaces (Fig. 10d, e). While small transmissivity changes during each cycle could stem from relatively open aperture fields (Fig. 10d, e), the more pronounced changes between cycles could



result from larger contact point stresses that could result in asperity failure and wear product removal.

The transmissivity for mated and offset fractures is always larger after the first cycle than after subsequent cycles (Fig. 13b), and the general trend is a decrease in transmissivity from the first cycle (smallest circle) to the last cycle (largest cicle). The finding of no significant increase in transmissivity after initial shear displacements (i.e., 1 mm, see Fig. 13) is congruent with previous findings by Kim and Inoue (2003) and Esaki et al. (1999).

In most cases, the transmissivity decrease after the first cycle is considerably larger then decreases for later cycles, which agrees with the previous literature on fracture closure and hydraulic aperture changes during repeated loading (Witherspoon et al. 1980; Gentier et al. 2013). This illustrates the importance of reservoir history on expected reservoir performance. Repeated fluid injection under high pressures leads to fracture opening, which can potentially cause a redistribution of gouge material along the main flow paths. Lowering of injection pressure may cause asperities and gouge material to be further comminuted, which could close flow pathways.

#### 4.2 Aperture Changes

Changes in mechanical and hydraulic aperture from the initial values at 1 MPa confining stress are shown in Fig. 5a–d, while changes in mechanical aperture versus effective confining stress are shown in Fig. 6a–d. Note that here one marker symbol ( $\triangleright$  and  $\triangleleft$  for increasing and decreasing confining pressure, respectively) represents an increase in confining stress of 1 MPa (up to 10 MPa confining stress) or 2.5 MPa (between 10 and 68 MPa confining stress), respectively. Generally, changes in  $a_{mech}$  are more drastic than those for  $a_{hyd}$  for all tests. Similar to the changes in transmissivity (Figs. 4a–e, 6a–d), aperture changes display hysteretic behavior. Generally, changes in mechanical and hydraulic aperture are larger during decreasing effective confining stress (Figs. 5a–d, 6a–d).

Mechanical and hydraulic aperture changes in tests 1, 7 and 10 can be categorized similarly (Fig. 5a, c, d). For low confining stresses, mechanical aperture changes increase strongly (Figs. 6a–d, 5a–d) until aperture changes (equivalent to aperture closure) increase monotonically (Fig. 6a, c, d) or converge against a constant value (Fig. 6b).

During initial mechanical aperture changes, the hydraulic aperture remains relatively unaffected, but changes strongly once initial mechanical aperture change has occurred (Fig. 5a–d). This change in behavior occurs between mechanical aperture changes between 0.15 and 0.25 mm (test 1), 0.5 and 0.6 mm (test 7) and 0.1 and 0.2 mm (test 10)  $a_{\rm mech}$ . The sudden decrease of  $a_{\rm hyd}$  could

be caused by the transition from uniform flow through most of the fracture to channelized flow. Hydraulic aperture changes become smaller after this increase in  $a_{hvd}$  change despite mechanical aperture changes increasing further with effective confining stress (Fig. 6a, c, d). This behavior can be explained by fluid flow confined to individual flow channels, which are not closed despite further increase in mechanical aperture changes. Once the maximum confining stress is reached and confining pressure is lowered again, the mechanical aperture  $a_{\text{mech}}$  change reverts slower than during initial loading (Fig. 6a-d). However, when comparing changes in  $a_{\text{mech}}$  to  $a_{\text{hyd}}$  (Fig. 5a, c, d), the mechanical aperture change recovers much faster than the hydraulic aperture change after peak loading. With fluid flow potentially concentrated within single channels, increasing  $a_{\text{mech}}$  (i.e., decreasing  $a_{\text{mech}}$  changes) would not lead to a redistribution of fluid flow since the contact area of the fracture surface is where the initial comminution of asperities and the resulting formation of gouge material would be located. Once  $a_{mech}$  opens sufficiently for the failed asperties to be flushed from the system,  $a_{hvd}$ decreases significantly between a change in the mechanical aperture of 0.2 and 0.4 mm. Mechanical aperture changes do not decrease more rapidly during that regime (Fig. 6ad), since the gouge material is only flushed from the system if compressive stresses on the gouge material are low and therefore do not significantly contribute to the continued propping of fractures. The rapid decrease in flow channels for confining stress increases up to 10 MPa is consistent with prior observations by Gentier et al. (2013).

#### 4.3 Analysis of Gouge Material

Grain size distribution of the comminution products (Fig. 7) organizes in two different families with a more pronounced log-normal distribution for tests 5, 11 and 12 than for tests 6, 7, 8, 9 and 10. Tests 5, 11 and 12 have small shear offsets (2, 1 and 1 mm, respectively), making the breakout of monominerals much more likely than in the other specimens, where large shear offsets lead to isolated contact points that can cause more rupturing of asperities during each loading cycle. With ongoing surface damage, the number of contact points may be increased until the local contact stress is then insufficient to overcome the asperity strength. This hypothesis is consistent with the analysis of mechanical and hydraulic aperture changes in Sect. 4.2.

#### 4.4 Surface Scans

Figures 8 and 9 compare the surfaces before and after testing and show strong alterations in the surfaces, but not



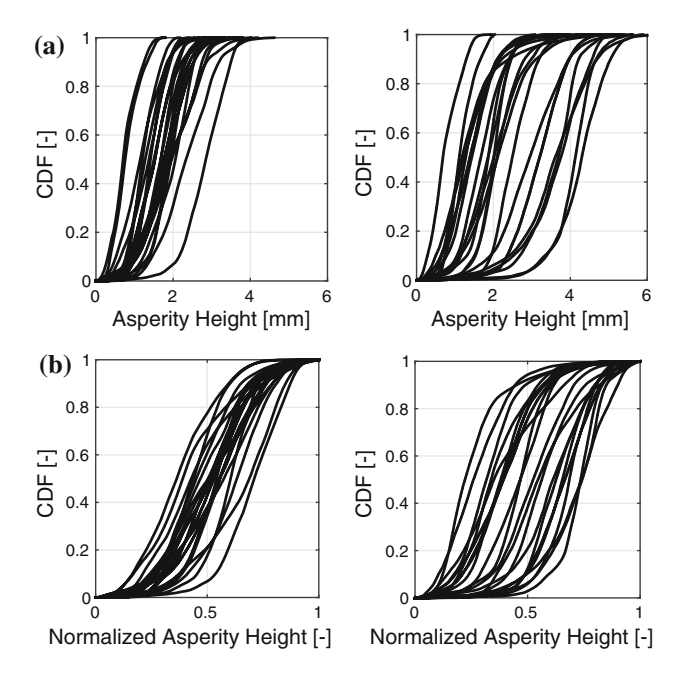


**Fig. 11** CDF of asperity height (**a**) and asperity height normalized to the maximum asperity height (**b**) for specimens 1–12 for fracture sides A and B before (*left*) and after (*right*) testing

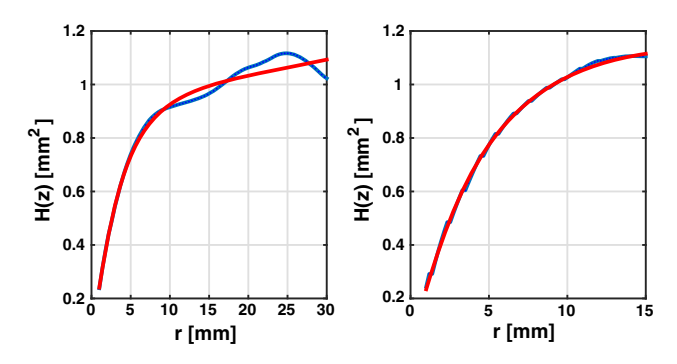


Fig. 12 Example of the correlation length function in x- (*left*) and y-direction (*right*) for specimen surface side A of test 6

decreasing asperity height during testing for all specimens (Fig. 14). Due to the small length scale of the fractures under investigation, the breaking of individual grains and asperities can lead to fractures that fill with gouge material, but do not develop better correlation between the two sides than before testing. This phenomenon is influenced by the displacement of the two fracture surfaces against each other. Displacement offsets of a few millimeters may lead to more point loads than in mated specimens (Fig. 10a–e), which can cause higher stresses in grains and asperities that can lead to failure, as mentioned above. The relationship between the decrease in contact area upon displacement can be related to the correlation length in the *x*-direction (Table 3), which influences the dilatancy of the fracture surfaces upon shear displacement.

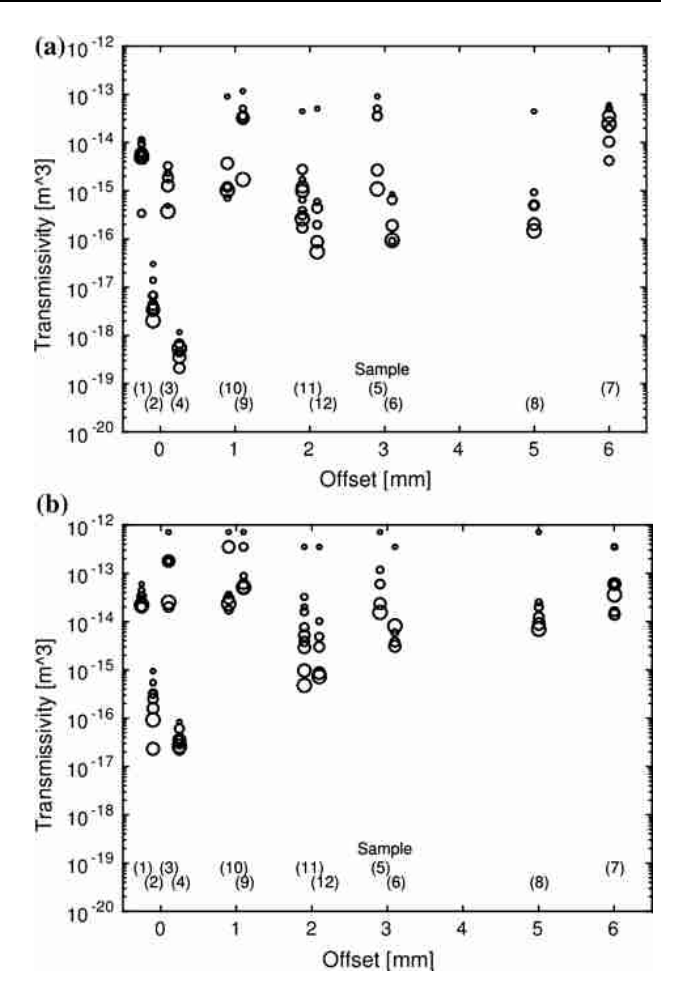
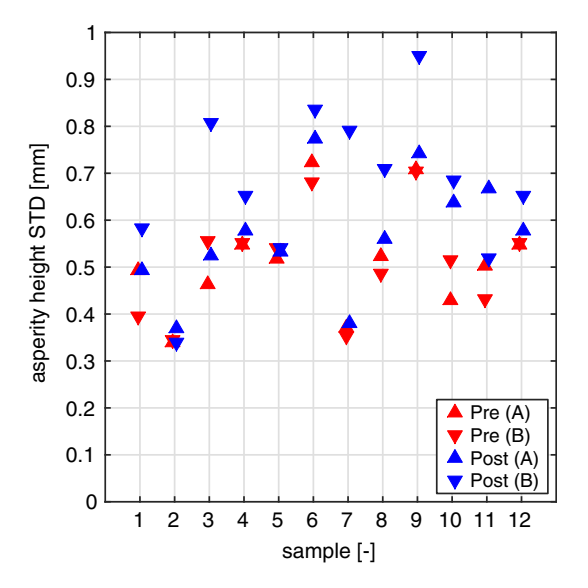


Fig. 13 Transmissivity values for all normal loads versus specimen offset for all specimens. Shown is one marker for each load cycle at: a maximum effective confining stress and b 1 MPa confining stress at the end of each load cycle. Cyclic loading progresses from the first cycle (*smallest circle*) to the last cycle (*largest circle*)

The large correlation lengths indicated in Table 3 could suggest that mechanical apertures should continually increase even for large shear displacements. However, most specimens show a strong increase of the correlation function H in the first few millimeters of specimen offset (e.g., Fig. 12), with convergence only occurring for large correlation lengths beyond the specimen scale. This indicates that the correlation decreases strongly during the first few millimeters of shear displacement and has no large effect for displacements larger than 5 or 10 mm as the correlation length has not converged yet. While the correlation length can be used as an indicator after which shear displacement of an offset specimen will not see an aperture increase anymore, it cannot be used to estimate the amount of contact area for a given displacement, which is what ultimately effects contact stresses between the two specimen sides. The contact area plays a very significant role since this determines the likelihood of surface damage in





**Fig. 14** Comparison of the standard deviation of asperity height on the surfaces A and B before (*red marker*) and after testing (*blue marker*) (color figure online)

the fracture for a given normal load, which can counteract changes in mechanical aperture caused by an increase in offset of a millimeter or two more. Therefore, we deduce that the correlation length is only a suitable metric to determine transmissivity in fractures for the first few millimeters of shear offset, with the amount of contact area being more significant for defining the important role of fracture damage under high normal loads.

Figure 11 shows a wider distribution of asperity heights after testing when comparing the values for the CDF at 0.5 and 1.0. While all but two fracture surfaces in Fig. 11a (left) have a maximum asperity height of 2 mm for the midpoint of the CDF before testing, more than half of all specimens surpasses this value for fracture surfaces after testing. Asperity height distributions across specimens show (Fig. 11) that maximum asperity height differences become more pronounced after testing, showing larger maximum values for asperity height and a weaker resemblance of the CDF between individual specimens. The effect of increased local normal stresses observed in Fig. 11a and b (e.g., Fig. 9c–e with strong surface changes) shows that repetitive loading does not necessarily lead to smoothed out asperity distributions and surfaces. While a few specimen surfaces became more homogeneous, it was observed on tests on offset specimens that cracks formed as a consequence of normal loading and the associated surfaces were fairly rough. Such cracks are shown in Fig. 9c (on surface B) where a crack parallel to the y-direction is visible at an x value of around 20 mm and in Fig. 9e (on surface A) where a crack parallel to the y-direction is visible at an x value of around 10 mm. Mineral inclusions of quartz and felspar in granodiorite have a high strength, which makes crack propagation more likely to occur at the boundaries with lower strength in between grains. Grain boundaries and grain size will then dominate the effect of surface deformation after increases in confining stress. Iwano and Einstein found evidence that asperity distribution in tensile fractures strongly depends on the overall grain size (Iwano and Einstein, 1993). Mineral grain sizes of intact core material were estimated to be between 2 and 7 mm, which can explain the large asperity heights after testing (Fig. 11b).

These findings indicate the influence of surface damage on fracture transmissivity, especially for fractures that experienced shear offset. Gouge production induced by surface damage can strongly counteract the transmissivity increase produced by shear offset (Figs.12, 13, 14).

#### 5 Conclusions

Granodiorite specimens with natural tensile and shear fractures were subjected to cyclic loading between 1 and 68 MPa confining pressure. Constant fluid flow rates through the specimen were established, which made it possible to measure the fluid pressure response to confining pressure. A total of 12 tests were performed, with four specimens tested in a mated configuration and eight specimens tested with shear displacement between 1 and 6 mm. Fracture surfaces were scanned before and after testing to give insight into surface deformation during testing. The gouge material produced by asperity damage was collected to study the impact of a gouge layer on transmissivity.

While all specimens showed a decrease in transmissivity with increased confining pressure, transmissivity decrease in mated and offset specimens shows fundamentally different behavior. Mated specimens only show strong decrease during individual load cycles for small confining pressures, suggesting fluid flow confined to channels for high confining pressures. Offset specimens show significant transmissivity decrease between load cycles and surface damage which leads to gouge production. Permeability generally decreased with ongoing loading cycles, indicating nonelastic deformation of the fracture surfaces. Specimens 2, 4, 7 and 10 showed hysteretic effects during individual loading cycles, with lower permeabilities during unloading of the specimen for respective effective confining pressures. During testing, the normal loads were large enough to keep most gouge material in place, which led to increased fluid pressures to sustain constant flow rates. It is hypothesized that breaking asperities, which are only flushed out of the system during decreasing normal loads, contribute strongly to the hysteretic transmissivity behavior observed during tests.



Mechanical and hydraulic aperture changes are compared, showing more pronounced changes in the mechanical aperture for all tests. Mechanical apertures change most drastically for low confining stresses. The most pronounced changes in hydraulic apertures occur after initial mechanical aperture closure can be observed. This could be explained by mechanical aperture closure causing fluid flow displacement to individual flow channels. This behavior changes again for high confining pressures, when mechanical aperture changes (i.e., closes) further while the hydraulic aperture does not change significantly. These nonlinear changes in the relationship of mechanical and hydraulic aperture changes can be attributed to increased surface damage and fracture closure for high confining pressures, while fluid flow is already confined to channel flow and is not strongly affected by compression of the fracture.

This work illustrates the importance of fatigue behavior, which is especially crucial for EGS with reservoir operation times of multiple decades. During operation of a reservoir, interruption of injection wells can lead to cyclic lowering and raising of the effective normal stress that fractures are subjected to. On the laboratory scale, this study shows differences of up to three orders of magnitude of the transmissivity, which suggests that the history of the fracture surfaces in a reservoir plays a significant role in the evolution of fracture transmissivity after initial stimulation.

Acknowledgments The authors want to thank two anonymous reviewers for their constructive suggestions which helped to improve this work. The authors further want to thank the National Cooperative for the Disposal of Radioactive Waste (Nagra), Switzerland, and the CRIEPI fractured rock study Takana et al. (2014) for providing us with the specimen material for our study. The authors further want to thank the chair of geosensors and engineering geodesy at ETH Zurich for their support with the photogrammetry scanner. This work was partially supported by the GEOTHERM II project, which is funded by the Competence Center Environment and Sustainability of the ETH Domain. This project benefitted from partial funding from DOE DE-FE0023354.

# References

- Barton N, Bandis S, Bakhtar K (1985) Strength, deformation and conductivity coupling of rock joints. Int J Rock Mech Min Sci 22(3):121–140
- Brown SR (1987) Fluid-flow through rock joints—the effect of surface-roughness. J Geophys Res-Solid Earth Planets 92(B2):1337–1347
- Chen Z, Narayan S, Yang Z, Rahman S (2000) An experimental investigation of hydraulic behaviour of fractures and joints in granitic rock. Int J Rock Mech Min Sci 37(7):1061–1071
- Cook NGW (1992) Natural joints in rock\*—mechanical, hydraulic and seismic behavior and properties under normal stress. Int J Rock Mech Min Sci Geomech Abstr 29(3):198–223
- Durham WB, Bonner BP (1994) Self-propping and fluid-flow in slightly offset joints at high effective pressures. J Geophys Res-Solid Earth 99(B5):9391–9399

- Esaki T, Hojo H, Kimura T, Kameda N, Deut Gesell E, Grundbau (1991) Shear-flow coupling test on rock joints. In: Proceedings—seventh international congress on rock mechanics, vol 1. Rock mechanics and environmental protection
- Esaki T, Du S, Mitani Y, Ikusada K, Jing L (1999) Development of a shear-flow test apparatus and determination of coupled properties for a single rock joint. Int J Rock Mech Min Sci 36(5):641–650
- Evans KF (2005) Permeability creation and damage due to massive fluid injections into granite at 3.5 km at soultz: 2. critical stress and fracture strength. J Geophys Res Solid Earth 110(B4):1–14
- Gentier S, Hopkins D, Riss J (2013) Role of fracture geometry in the evolution of flow paths under stress. In: Faybishenko B, Witherspoon PA, Benson SM (eds) Dynamics of fluids in fractured rock, American Geophysical Union, pp 169–184. doi:10.1029/GM122p0169
- Hakami E, Larsson E (1996) Aperture measurements and flow experiments on a single natural fracture. Int J Rock Mech Min Sci Geomech Abstr 33(4):395–404
- Hakami, E and Einstein, H H and Gentier, S and Iwano, M (1993) Characterisation of fracture apertures-Methods and parameters. 8th ISRM congress 1995
- Iwano M, Einstein H (1993) Stochastic analysis of surface roughness, aperture and flow in a single fracture. In: Proceedings of the ISRM International Symposium Eurock '93. Lisbon. pp 135–1441
- Kim HM, Inoue J (2003) Analytical approach for anisotropic permeability through a single rough rock joint under shear deformation. J Geophys Res Solid Earth 108(8):5-1–5-10
- Lee HS, Cho TF (2002) Hydraulic characteristics of rough fractures in linear flow under normal and shear load. Rock Mech Rock Eng 35(4):299–318. doi:10.1007/s00603-002-0028-y
- Li B, Jiang Y, Koyama T, Jing L, Tanabashi Y (2008) Experimental study of the hydro-mechanical behavior of rock joints using a parallel-plate model containing contact areas and artificial fractures. Int J Rock Mech Min Sci 45(3):362–375
- Li Y, Chen Y, Zhou C (2014) Hydraulic properties of partially saturated rock fractures subjected to mechanical loading. Eng Geol 179:24–31
- Louis C (1969) A study of groundwater flow in jointed rock and its influence on the stability of rock masses. Rock mechanics research, report 10
- McClure M, Horne R (2014) Characterizing hydraulic fracturing with a tendency-for-shear-stimulation test. Spe Reserv Eval Eng 17(2):233–243
- Oron AP, Berkowitz B (1998) Flow in rock fractures: the local cubic law assumption reexamined. Water Resour Res 34(11):2811–2825. doi:10.1029/98wr02285
- Park H, Osada M, Matsushita T, Takahashi M, Ito K (2013) Development of coupled shear-flow-visualization apparatus and data analysis. Int J Rock Mech Min Sci 63:72–81. doi:10.1016/j. ijrmms.2013.06.003
- Pyrak-Nolte LJ, Morris JP (2000) Single fractures under normal stress: the relation between fracture specific stiffness and fluid flow. Int J Rock Mech Min Sci 37(1–2):245–262. doi:10.1016/s1365-1609(99)00104-5
- Raven KG, Gale JE (1985) Water-flow in a natural rock fracture as a function of stress and sample-size. Int J Rock Mech Min Sci 22(4):251–261
- Renshaw CE (1995) On the relationship between mechanical and hydraulic apertures in rough-walled fractures. J Geophys Res-Solid Earth 100(B12):24,629–24,636. doi:10.1029/95jb02159
- Rutqvist J, Stephansson O (2003) The role of hydromechanical coupling in fractured rock engineering. Hydrogeol J 11(1):7–40
- Shugang W, Elsworth D, Jishan L (2013) Mechanical behavior of methane infiltrated coal: the roles of gas desorption, stress level



- and loading rate. Rock Mech Rock Eng 46(5):945–958. doi:10. 1007/s00603-012-0324-0
- Takana Y, Miyakawa K, Fukahori D, Kiho K, Goto K (2014) Survey of flow channels in rock mass fractures by resin injection. Asian rock mechanics symposium 8
- Tester JW, Anderson BJ, Batchelor AS, Blackwell DD, DiPippo R, Drake EM, Garnish J, Livesay B, Moore MC, Nichols K, Petty S, Toksöz MN, Veatch RW, Baria R, Augustine C, Murphy E, Negraru P, Richards M (2006) The Future of geothermal energy; impact of enhanced geothermal systems (EGS) on the United States in the 21st century. Technical report INL/EXT-06-11746, Idaho National Laboratory
- Walsh JB (2003) A theoretical analysis of sliding of rough surfaces. J Geophys Res-Solid Earth 108(B8). doi:10.1029/2002jb002127
- Wang S, Elsworth D, Liu J (2011) Permeability evolution in fractured coal: the roles of fracture geometry and water-content. Int J Coal Geol 87(1):13–25
- Witherspoon PA, Wang JSY, Iwai K, Gale JE (1980) Validity of cubic law for fluid-flow in a deformable rock fracture. Water Resour Res 16(6):1016–1024
- Xiong X, Li B, Jiang Y, Koyama T, Zhang C (2011) Experimental and numerical study of the geometrical and hydraulic

- characteristics of a single rock fracture during shear. Int J Rock Mech Min Sci 48(8):1292–1302
- Yeo IW, De Freitas MH, Zimmerman RW (1998) Effect of shear displacement on the aperture and permeability of a rock fracture. Int J Rock Mech Min Sci 35(8):1051–1070
- Zhong Z, Elsworth D, Hu Y (2014) Evolution of strength and permeability in stressed fractures with fluid-rock interactions. Pure Appl Geophys 173(2):525–536. doi:10.1007/s00024-015-1099-5
- Zhu WC, Liu J, Elsworth D, Polak A, Grader A, Sheng JC, Liu JX (2007) Tracer transport in a fractured chalk: X-ray ct characterization and digital-image-based (dib) simulation. Transport Porous Media 70(1):25–42
- Zimmerman RW, Kumar S, Bodvarsson GS (1991) Lubrication theory analysis of the permeability of rough-walled fractures. Int J Rock Mech Min Sci Geomech Abstr 28(4):325–331
- Zimmerman RW, Bodvarsson GS (1996) Hydraulic conductivity of rock fractures. Transport Porous Media 23(1):1–30

